A study of harmonic spatial propagation along AC power lines of meshed power systems

Liu, Chengxi; Zhen , Gong; Silva, Filipe Miguel Faria da; Lai, Qiupin ; Hu, Pan

Published in:
IET Circuits, Devices & Systems

DOI (link to publication from Publisher):
10.1049/cds2.12107

Publication date:
2022

Document Version
Publisher's PDF, also known as Version of record

Received: 21 December 2020 | Revised: 15 April 2021 | Accepted: 29 November 2021

DOI: 10.1049/cds2.12107

IET Circuits, Devices & Systems

The Institution of Engineering and Technology WILEY

ORIGINAL RESEARCH

A study of harmonic spatial propagation along AC power lines of meshed power systems

Chengxi Liu[1] | Zhen Gong[1] | Filipe Faria da Silva[2] | Qiupin Lai[1] | Pan Hu[3]

[1]School of Electrical Engineering and Automation, Wuhan University, Wuhan, China

[2]Department of Energy Technology, Aalborg University, Aalborg, Denmark

[3]Hubei Electric Power Research Institute, Wuhan, China

Correspondence

Chengxi Liu, School of Electrical Engineering and Automation, Wuhan University, Room 3402, Wuhan, China.
Email: liuchengxi@whu.edu.cn

Funding information

National Natural Science Foundation of China, Grant/Award Number: 52007133

Abstract

Severe harmonics propagation in power systems may result in increased power losses and equipment damages. In this paper, an elliptic formula is derived to analyse the harmonic spatial distribution not only at the substations but also along the power lines or cables and to give a system-wide overview of harmonic levels. It is observed that harmonic distortion along power lines can be higher than that at the busbars and the maximum amplitude of harmonic voltage and current denoted as weak positions along power lines depends on the steady-state harmonic angle difference of voltage and current at busbars, the length of power lines, and the harmonic order. All cases are modelled in detail by analytical geometry and analysed in MATLAB. In this regard, a method to identify the weak positions in terms of maximum harmonic levels in a power system is presented, and its corresponding harmonic orders are determined. The accuracy of the model is tested using time-domain simulations in PSCAD/EMTDC.

KEYWORDS

harmonic distortion, harmonics suppression

1 | INTRODUCTION

The ever-increasing amount of renewable energies in the power grid is pushing the reinforcement of the transmission and distribution systems, to avoid overloading of system equipment. In some countries, such as Denmark, Sweden and Germany, there are interests of reinforcing parts of the transmission system by installing underground cables (UGCs), rather than overhead lines (OHLs) [1].

The implementation of high-voltage UGCs can cause serious issues regarding excess harmonic levels in the grid violating the upper limitations of international standards or grid codes [2], which is set to protect the system components and maintain the system integrity. One of the main differences between UGCs and OHLs is that the same length of UGCs has significantly larger shunt capacitance than that of OHLs [3]. A high-voltage UGC has its shunt capacitance 20–50 times larger than an equivalent OHL with the same length, resulting in much lower resonant frequencies, at which the harmonic voltage or harmonic current might be significantly amplified [4]. There are thus potential risks of harmonic problem when implementing high-voltage UGCs in the transmission systems [5].

Low frequency resonance is a challenging issue in terms of keeping harmonic voltage below the planning level. Small harmonic injections from non-linear apparatus may result in large harmonic voltage and current magnitude along power lines [6], which complicate harmonic distortion estimation and the design of mitigation solutions. For example, a high proportion of HVAC cables in offshore wind farms leads to temporary overvoltage (TOV) and low frequency resonances [7, 8], and problems of low order resonances for meshed system is analysed in Refs. [9, 10]. Also, the integration of power electronics devices, such as LCC-HVDC, brings further harmonic sources that can excite local and remote resonances in the power systems. Therefore, the harmonic assessment and harmonic mitigation in power systems are becoming more and more important.

Reference [11] proposes an index to quantify the harmonic propagation areas and amplification characteristic, and References [12, 13] introduce a location method of the severe resonance point. Reference [14] proposes a harmonic propagation measurement method regarding harmonic amplitude and phase. Reference [15] analyses the propagation mechanism and concludes that the distribution characteristics of

harmonic voltage and Total Harmonic Distortion (THD) in distribution networks are decided by the injection points of DGs; however, lumped models of power lines without accurate high-frequency parameter are used, and the distribution of harmonic voltage inside the power lines is ignored. Also, whether the conclusion is suitable for transmission grids and which harmonic orders are affected by DG are not discussed yet. This paper can fill this gap by analysing the distribution of harmonics along power lines that could lead to overvoltage or overcurrent problems within it. Telegrapher's equations have been early proposed in References [16–18] that the voltage and current spatial propagation are characterised. These equations are utilised as the basis of ellipse formulae in this paper, however, the elliptical relationship between voltage and current along the power line and the impact factors of the different shapes of ellipses have not been analysed, from which, one can obtain the relationship between peak voltage and peak current along a power line. Heuristic algorithm, such as GA, ant lion or spider monkey optimisation, is utilised for minimisation of total real power loss or optimal allocation problems in the renewable distribution generators integrated system in Refs. [19, 20], which might be the novel ways to study the harmonic problems in power-electronics-integrated power systems. These methods could be utilised in solving the problems of optimised filter allocation considering harmonic amplification along power lines which is the future work of this paper. Nowadays, little research has been focussed on the spatial distribution of harmonics, especially along the power lines, where harmonic distortion may not conform to the standards or grid codes. The harmonic levels within the overhead lines and the cables in a power system, shown in Figure 1, might be much higher than the harmonic levels measured at the busbars when harmonic resonant points are inside the power lines.

This paper gives the analytical expressions for harmonic spatial distribution over the power systems using an analytical geometry model. The expressions are then verified by time-domain simulations. The main contributions are in threefold: First, the harmonic propagation in a general meshed system is studied. The harmonic levels are calculated not only in busbars but also along the power lines, and an analytical geometry model, ellipse formula, is derived to represent the harmonic spatial distribution along power lines. Second, three main impact factors that influence the shapes of ellipse are discussed in detail: harmonic orders, power line lengths and phase angle differences of harmonic voltage and current measured at one terminal of power lines. It is discovered that higher amplifications could occur in longer lines, and more likely at higher frequency ranges when phase angle differences are close to 90° or 270°. Third, the paper proposes a method of identifying weak positions of harmonic voltages and currents along the power lines. All analyses are based on the analytical geometry models derived in MATLAB and verified on two benchmark systems in PSCAD.

The weak position proposed here is referred to peak magnitudes of harmonic voltages and currents in different orders that beyond harmonic levels. In this paper, the asymmetry and interphase mutual inductance are not considered. Only uniform transmission lines are considered in which the circuit parameters are uniformly distributed.

The rest of the paper is organised as follows. Section 2 explains the elliptic formula for harmonic propagation. Section 3 analyses the harmonic propagation using the proposed elliptic formulation and proposes a method to identify weak positions along power lines that could be over the limits of standards. Section 4 uses a 12-bus and IEEE 39-bus system to verify the harmonic propagation formula and the identified weak position. Finally, conclusions are drawn in Section 5.

2 | FORMULAE OF HARMONIC PROPAGATION ALONG TRANSMISSION LINES

2.1 | Elliptic formulae of U-I magnitude

As shown in Figure 2, a uniform transmission line can be modelled as infinite number of series-connected sections composed of infinitesimal series impedance, that is $(r_0 + j\omega L_0)dx$, and shunt admittance, that is $(g_0 + j\omega C_0)dx$. $\mathbf{U}_1$, $\mathbf{I}_1$, and $\mathbf{U}_2$, $\mathbf{I}_2$ are the measurable voltage and current vectors at both terminals, that is Bus 1 and Bus 2, respectively. $\mathbf{U}(x)$ and $\mathbf{I}(x)$

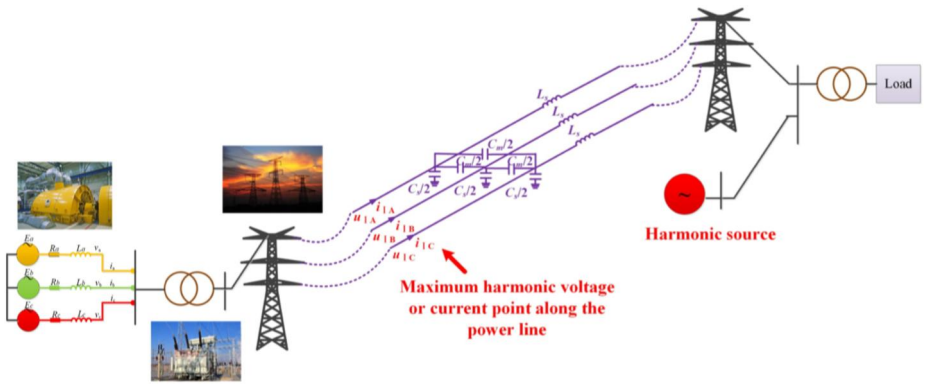

FIGURE 1 Harmonic distribution along a power line

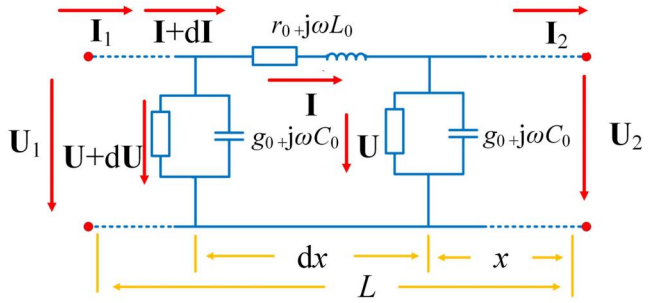

FIGURE 2 Distributed model of a power line

are the voltage and current vectors inside the power line, with a distance of x from Bus 2. The voltage drop on each section is

$$d\mathbf{U}(x) = \mathbf{I}(x)(r_0 + \mathrm{j}\omega L_0)dx \tag{1}$$

and the current flowing in the shunt admittance is

$$d\mathbf{I}(x) = (\mathbf{U}(x) + d\mathbf{U})(g_0 + \mathrm{j}\omega C_0)dx \tag{2}$$

Then,

$$\frac{d^2\mathbf{U}(x)}{dx^2} = (g_0 + \mathrm{j}\omega C_0)(r_0 + \mathrm{j}\omega L_0)\mathbf{U}(x) \tag{3}$$

So, complex-valued voltage and current depending on the distance x, that is $\mathbf{U}(x)$ and $\mathbf{I}(x)$ can be calculated as (4) shown, where γ is the complex propagation coefficient, and Z_c is the characteristic impedance shown in Equation (5).

$$\begin{cases} \mathbf{U}(x) = \dfrac{1}{2}(\mathbf{U}_2 + Z_c\mathbf{I}_2)e^{\gamma x} + \dfrac{1}{2}(\mathbf{U}_2 - Z_c\mathbf{I}_2)e^{-\gamma x} \\ \mathbf{I}(x) = \dfrac{1}{2Z_c}(\mathbf{U}_2 + Z_c\mathbf{I}_2)e^{\gamma x} - \dfrac{1}{2Z_c}(\mathbf{U}_2 - Z_c\mathbf{I}_2)e^{-\gamma x} \end{cases} \tag{4}$$

$$\gamma = \sqrt{(g_0 + \mathrm{j}\omega C_0)(r_0 + \mathrm{j}\omega L_0)} = \alpha + \mathrm{j}\beta$$

$$Z_c = \sqrt{\frac{r_0 + \mathrm{j}\omega L_0}{g_0 + \mathrm{j}\omega C_0}} = R_c + \mathrm{j}X_c = |Z_c|e^{\mathrm{j}\theta_c} \tag{5}$$

Proposition I *For a lossless power line, the real part of* $\mathbf{U}(x)$ *and imaginary part* $\mathbf{I}(x)$ *follow an elliptic formula along the power line (vary with* x*), so do the imaginary part of* $\mathbf{U}(x)$ *and real part of* $\mathbf{I}(x)$.

Proof: The series resistance r_0 and shunt conductance g_0 of a lossless power line are not considered, so (5) can be derived to (6).

$$\gamma = \mathrm{j}\beta = \mathrm{j}\omega\sqrt{L_0C_0}$$

$$Z_c = R_c = \sqrt{L_0/C_0} \tag{6}$$

Then, (4) can be transformed to (7), where $\mathbf{U}(x)$ and $\mathbf{I}(x)$ are represented as a combination of sinusoidal functions.

$$\begin{cases} \mathbf{U}(x) = \mathbf{A}\cos(\beta x) + \mathbf{B}\sin(\beta x) \\ \mathbf{I}(x) = \mathbf{C}\cos(\beta x) + \mathbf{D}\sin(\beta x) \end{cases} \tag{7}$$

where **A**–**D** are complex-valued coefficients expressed below:

$$\begin{cases} \mathbf{A} = \mathbf{U}_2 \\ \mathbf{B} = \mathrm{j}Z_c\mathbf{I}_2 \end{cases} \text{and} \begin{cases} \mathbf{C} = \mathbf{I}_2 \\ \mathbf{D} = \mathrm{j}(\mathbf{U}_2/Z_c) \end{cases} \tag{8}$$

An elliptic formula (10) can be used to describe the relationship between vectors of $\mathbf{U}(x)$ and $\mathbf{I}(x)$ based on (9):

$$\begin{cases} \mathbf{U}(x) = \sqrt{\mathbf{A}^2 + \mathbf{B}^2}\sin(\beta x + \varphi), \ \tan\varphi = \dfrac{\mathbf{A}}{\mathbf{B}} \\ \mathbf{I}(x) = \sqrt{\mathbf{C}^2 + \mathbf{D}^2}\cos(\beta x - \varphi'), \ \tan\varphi' = \dfrac{\mathbf{D}}{\mathbf{C}} = -\tan\varphi, \varphi = -\varphi' \end{cases} \tag{9}$$

$$\frac{[\mathbf{I}(x)]^2}{\mathbf{C}^2 + \mathbf{D}^2} + \frac{[\mathbf{U}(x)]^2}{\mathbf{A}^2 + \mathbf{B}^2} = 1 \tag{10}$$

Utilities are more concerned about the magnitudes of harmonics, but **U-I** magnitude along x cannot be directly obtained by (10), because **A**, **B**, **C**, **D**, $\mathbf{U}(x)$ and $\mathbf{I}(x)$ are all complex values.

Firstly, the relationship of real parts, imaginary parts and amplitudes of $\mathbf{U}(x)$ and $\mathbf{I}(x)$ are proven to subject to elliptic formulae.

Let $\mathbf{U}(x) = \Re\mathbf{U}(x) + j\Im\mathbf{U}(x)$, $\mathbf{I}(x) = \Re\mathbf{I}(x) + j\Im\mathbf{I}(x)$, where $\Re(\cdot)$ and $\Im(\cdot)$ are real and imaginary operators. In this case, real part of $\mathbf{U}(x)$ and imaginary part of $\mathbf{I}(x)$ are

$$\begin{aligned} \Re\mathbf{U}(x) &= \Re(\mathbf{U}_2)\cos(\beta x) - Z_c\Im(\mathbf{I}_2)\sin(\beta x) \\ &= \sqrt{\Re(\mathbf{U}_2)^2 + Z_c{}^2\Im(\mathbf{I}_2)^2}\sin(\beta x - \varphi_1), \\ \tan\varphi_1 &= \frac{\Re(\mathbf{U}_2)}{Z_c\Im(\mathbf{I}_2)} \\ \Im\mathbf{I}(x) &= \Im(\mathbf{I}_2)\cos(\beta x) + \frac{\Re(\mathbf{U}_2)}{Z_c}\sin(\beta x) \\ &= \sqrt{\frac{\Re(\mathbf{U}_2)^2}{Z_c{}^2} + \Im(\mathbf{I}_2)^2}\cos(\beta x - \varphi_2), \\ \tan\varphi_2 &= \frac{\Re(\mathbf{U}_2)}{Z_c\Im(\mathbf{I}_2)} = \tan\varphi_1 \end{aligned} \tag{11}$$

From (11), the real part of $\mathbf{U}(x)$ and imaginary part of $\mathbf{I}(x)$ follow a real-valued elliptic formula shown in (12).

$$\frac{\Re^2(\mathbf{U})}{\Re(\mathbf{U}_2)^2 + Z_c{}^2\Im(\mathbf{I}_2)^2} + \frac{\Im^2(\mathbf{I})}{\frac{\Re(\mathbf{U}_2)^2}{Z_c{}^2} + \Im(\mathbf{I}_2)^2} = 1 \tag{12}$$

Similarly, the imaginary part of $\mathbf{U}(x)$ and real part of $\mathbf{I}(x)$ also follows a companion elliptic formula shown in (13).

$$\frac{\Im^2(\mathbf{U})}{\Im(\mathbf{U}_2)^2 + {Z_c}^2\Re(\mathbf{I}_2)^2} + \frac{\Re^2(\mathbf{I})}{\frac{\Im(\mathbf{U}_2)^2}{Z_c^2} + \Re(\mathbf{I}_2)^2} = 1 \tag{13}$$

Proposition II *For a lossless power line, magnitudes of voltage and current along the lines follow an elliptic formula about the distance to the terminal x.*

Proof: magnitudes of $\mathbf{U}(x)$ and $\mathbf{I}(x)$ are expressed by (14),

$$\begin{aligned} |\mathbf{U}(x)| &= \sqrt{(\Re\mathbf{U})^2 + (\Im\mathbf{U})^2} \\ &= \sqrt{a\cos^2(\beta x) + b\sin^2(\beta x) + c\cos(\beta x)\sin(\beta x)} \\ |\mathbf{I}(x)| &= \sqrt{(\Re\mathbf{I})^2 + (\Im\mathbf{I})^2} \\ &= \sqrt{d\cos^2(\beta x) + e\sin^2(\beta x) + f\cos(\beta x)\sin(\beta x)} \end{aligned} \tag{14}$$

where *a-f* are real-valued coefficients shown below:

$$\begin{cases} a = [\Re(\mathbf{A})]^2 + [\Im(\mathbf{A})]^2 = |\mathbf{A}|^2 \\ b = [\Re(\mathbf{B})]^2 + [\Im(\mathbf{B})]^2 = |\mathbf{B}|^2 \\ c = 2\Re(\mathbf{A})\cdot\Re(\mathbf{B}) + 2\Im(\mathbf{A})\cdot\Im(\mathbf{B}) \\ d = [\Re(\mathbf{C})]^2 + [\Im(\mathbf{C})]^2 = |\mathbf{C}|^2 \\ e = [\Re(\mathbf{D})]^2 + [\Im(\mathbf{D})]^2 = |\mathbf{D}|^2 \\ f = 2\Re(\mathbf{C})\cdot\Re(\mathbf{D}) + 2\Im(\mathbf{C})\cdot\Im(\mathbf{D}) \end{cases} \tag{15}$$

Then, (14) can be transformed to (16) with the coefficients *a–f* shown in (15).

$$\begin{aligned} |\mathbf{U}(x)|^2 &= a + (b-a)\sin^2(\beta x) + c\sqrt{1-\sin^2(\beta x)}\sin(\beta x) \\ |\mathbf{I}(x)|^2 &= d + (e-d)\sin^2(\beta x) + f\sqrt{1-\sin^2(\beta x)}\sin(\beta x) \end{aligned} \tag{16}$$

Using the following relationship in (17)

$$\begin{aligned} e - d &= (a-b)/{Z_c}^2 \\ f &= -c/{Z_c}^2 \end{aligned} \tag{17}$$

and substitute (17) into (16), Equation (18) is obtained,

$$\frac{|\mathbf{I}(x)|^2}{\left(\frac{a+b}{Z_c^2}\right)} + \frac{|\mathbf{U}(x)|^2}{a+b} = 1 \tag{18}$$

which proves that the magnitudes of $\mathbf{U}(x)$ and $\mathbf{I}(x)$ also follow elliptic formula. Note that, ω is the excitation frequency and parameters of a, b, and Z_c are all dependent on ω, so the elliptic formula, that is Equation (18), is not only applicable for fundamental frequency, but also for harmonic frequencies.

Key parameters of ellipses (focus points, semi-major axis, semi-minor axis and eccentricity) shown in Equations (12), (13), (18) are illustrated in Table 1. **U-I** figures are proposed to express the magnitude along the power line.

Proposition III *For a lossy line, magnitudes of* $\mathbf{U}(x)$ *and* $\mathbf{I}(x)$ *have distance-varying maximum value.*

Proof: Different from (4), if series resistance r_0 and shunt conductance g_0 are not neglected, $\mathbf{U}(x)$ and $\mathbf{I}(x)$ are derived by (19), where $\alpha \neq 0$

$$\begin{cases} \mathbf{U}(x) = \mathbf{A}\cos(\beta x - j\alpha x) + \mathbf{B}\sin(\beta x - j\alpha x) \\ \mathbf{I}(x) = \mathbf{C}\cos(\beta x - j\alpha x) + \mathbf{D}\sin(\beta x - j\alpha x) \end{cases} \tag{19}$$

Equation (19) can be rearranged as (20) where complex coefficients **A-D** are the same with (8).

For fundamental frequency or low order harmonic components with one quarter of wavelengths exceeding power line length, the corresponding maximum magnitudes of $\mathbf{U}(x)$ and $\mathbf{I}(x)$ are located at busbars at both ends of the line.

$$\begin{aligned} &\mathbf{U}(x) = \sqrt{\mathbf{A}^2 + \mathbf{B}^2}\sin(\beta x - j\alpha x + \varphi),\ \tan\varphi = \frac{\mathbf{A}}{\mathbf{B}} \\ &\mathbf{I}(x) = \sqrt{\mathbf{C}^2 + \mathbf{D}^2}\cos(\beta x - j\alpha x - \varphi'),\ \tan\varphi' = \frac{\mathbf{D}}{\mathbf{C}} = -\tan\varphi, \\ &\varphi = -\varphi' \end{aligned} \tag{20}$$

TABLE 1 Parameters of elliptic Equations (12), (13), (18)

	Ellipse		
Parameters	$\Re\mathbf{U}(x)$ - $\Im\mathbf{I}(x)$ **plot**	$\Im\mathbf{U}(x)$ - $\Re\mathbf{I}(x)$ **plot**	$\lvert\mathbf{U}(x)\rvert$ - $\lvert\mathbf{I}(x)\rvert$ **plot**
Focus points	$(0, \pm\sqrt{(1-1/Z_c^2)\Re(\mathbf{U}_2)^2 + (Z_c^2-1)\Im(\mathbf{I}_2)^2})$ Denoted as $(0, \pm f_1)$	$(0, \pm\sqrt{(1-1/Z_c^2)\Im(\mathbf{U}_2)^2 + (Z_c^2-1)\Re(\mathbf{I}_2)^2})$ denoted as $(0 \pm f_2)$	$(0, \pm\sqrt{(Z_c{}^2-1)/Z_c{}^2 \times (a+b)})$ denoted as $(0 \pm f_3)$
Semi-major axis	$\sqrt{\Re(\mathbf{U}_2)^2 + Z_c{}^2\Im(\mathbf{I}_2)^2}$ denoted as a_1	$\sqrt{\Im(\mathbf{U}_2)^2 + Z_c{}^2\Re(\mathbf{I}_2)^2}$ denoted as a_2	$\sqrt{a+b}$ denoted as a_3
Semi-minor axis	$\sqrt{\Re(\mathbf{U}_2)^2/Z_c^2 + \Im(\mathbf{I}_2)^2}$ denoted as b_1	$\sqrt{\Im(\mathbf{U}_2)^2/Z_c^2 + \Re(\mathbf{I}_2)^2}$ denoted as b_2	$\sqrt{a+b}/Z_c$ denoted as b_3
Eccentricity	$\frac{\sqrt{(1-1/Z_c^2)\Re(\mathbf{U}_2)^2 + (Z_c^2-1)\Im(\mathbf{I}_2)^2}}{\sqrt{\Re(\mathbf{U}_2)^2 + Z_c{}^2\Im(\mathbf{I}_2)^2}}$	$\frac{\sqrt{(1-1/Z_c^2)\Im(\mathbf{U}_2)^2 + (Z_c^2-1)\Re(\mathbf{I}_2)^2}}{\sqrt{\Im(\mathbf{U}_2)^2 + Z_c{}^2\Re(\mathbf{I}_2)^2}}$	$\sqrt{(Z_c{}^2-1)/Z_c{}^2 \times (a+b)}/\sqrt{a+b}$

For higher order components with the wavelengths shorter than power line lengths, it can be concluded that the maximum magnitudes of $\mathbf{U}(x)$ and $\mathbf{I}(x)$ along the transmission lines are dependent on the real part of propagation coefficient α and imaginary part of φ. If $\Im(\varphi) - \alpha < 0$, the peak harmonic voltage is located at the peak position closer to the sending end (x closer to L). Otherwise, the peak harmonic voltage is located on the peak position closer to the receiving end (x closer to 0).

2.2 | Discussion about the elliptic formulae

There are 3 types of ellipses: (1) The relationship between the real part of $\mathbf{U}(x)$ and the imaginary part of $\mathbf{I}(x)$ as shown in the second column of Table 1; (2) The relationship between the imaginary part of $\mathbf{U}(x)$ and the real part of $\mathbf{I}(x)$ as shown in the third column of Table 1; (3) Parameters of $|\mathbf{U}(x)|$-$|\mathbf{I}(x)|$ magnitude ellipse shown in Equation (18) is illustrated in the fourth column of Table 1. Ellipses are drawn in rectangular coordinate system and x axis represents $\Im\mathbf{I}(x)$, $\Re\mathbf{I}(x)$ and $|\mathbf{I}(x)|$ and y axis represents $\Re\mathbf{U}(x)$, $\Im\mathbf{U}(x)$ and $|\mathbf{U}(x)|$, respectively. All of these diagrams except for $|\mathbf{U}(x)|$-$|\mathbf{I}(x)|$ ellipse are shown in Figure 3.

For the discussion of $\mathbf{U}(x)$−$\mathbf{I}(x)$ magnitude plot, the first quadrant of $|\mathbf{U}(x)|$-$|\mathbf{I}(x)|$ ellipse is of concern since the magnitudes are always positive values. Furthermore, there are two different scenarios of the $|\mathbf{U}(x)|$-$|\mathbf{I}(x)|$ magnitude ellipse constrained by peak values of $|\mathbf{U}(x)|-|\mathbf{I}(x)|$ magnitude illustrated in Figure 4 below in accordance with different phase angles of harmonic injection: (i) The minimum values of voltage and current in a specific harmonic order are 0 and their peak values are the maximum quantities compared to the second scenario. The corresponding trajectory and phase angle are depicted as follows: First quadrant of the ellipse between $(|\mathbf{I}(x)|_{max1}, |\mathbf{U}(x)|_{min1})$ and $(|\mathbf{I}(x)|_{min1}, |\mathbf{U}(x)|_{max1})$ when $\angle\mathbf{U}_2$-$\angle\mathbf{I}_2 = 90° \pm k \times 180°$, $k = 0, 1, 2, 3, \ldots$; (ii) The minimum values of the harmonic components are non-zero quantities and the peak values are smaller than that of scenario before. The trajectory and phase angle are as follows: Part of first quadrant of the ellipse between $(|\mathbf{I}(x)|_{max2}, |\mathbf{U}(x)|_{min2})$ and $(|\mathbf{I}(x)|_{min2}, |\mathbf{U}(x)|_{max2})$ when $\angle\mathbf{U}_2$-$\angle\mathbf{I}_2 \neq 90° \pm k \times 180°$, $k = 0, 1, 2, 3, \ldots$, and both of them are depicted in Figure 4a,b, respectively, that $\angle\mathbf{U}_2$ and $\angle\mathbf{I}_2$ are phase angle of busbar voltage $\mathbf{U}_2$ and current $\mathbf{I}_2$.

Taking voltage magnitude $|\mathbf{U}(x)|$ along transmission line as an example, Equation (16) can be transformed to (21):

$$|\mathbf{U}(x)|^2 = a + \frac{1}{2}(b-a) + \sqrt{(0.5\times c)^2 + [0.5\times(b-a)]^2}\sin(2\beta x - \varphi) \tag{21}$$

where

$$\varphi = \arctan\left(\frac{b-a}{c}\right) \tag{22}$$

To obtain the peak value of $|\mathbf{U}(x)|$, the maximum c in Equation (21) needs to be calculated according to Equation (15) as Equations (23) and (24) shown when $\angle\mathbf{U}_2$-$\angle\mathbf{I}_2 = 90° \pm k \times 180°$, $k = 0, 1, 2, 3, \ldots$.

$$\begin{aligned} c &= 2\Re(\mathbf{U}_2)\Re(jZ_c \times \mathbf{I}_2) + 2\Im(\mathbf{U}_2)\Im(jZ_c \times \mathbf{I}_2) \\ &= 2Z_c(|\mathbf{U}_2|\sin(\theta_{\mathbf{U}_2}) \times |\mathbf{I}_2|\cos(\theta_{\mathbf{I}_2}) - |\mathbf{U}_2|\cos(\theta_{\mathbf{U}_2}) \\ &\quad \times |\mathbf{I}_2|\sin(\theta_{\mathbf{I}_2})) \\ &= 2Z_c|\mathbf{U}_2||\mathbf{I}_2|\sin(\theta_{\mathbf{U}_2} - \theta_{\mathbf{I}_2}) \end{aligned} \tag{23}$$

$$c_{max} = 2Z_c|\mathbf{U}_2||\mathbf{I}_2| \tag{24}$$

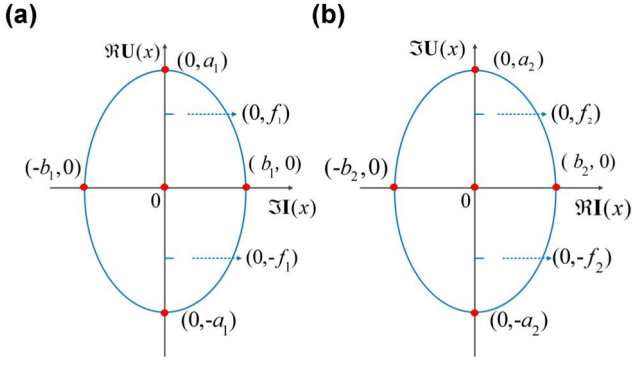

FIGURE 3 Ellipse diagram of Equations (12) and (14): (a) real part of U(x) and imaginary part of I(x), (b) imaginary part of $\mathbf{U}(x)$ and real part of $\mathbf{I}(x)$

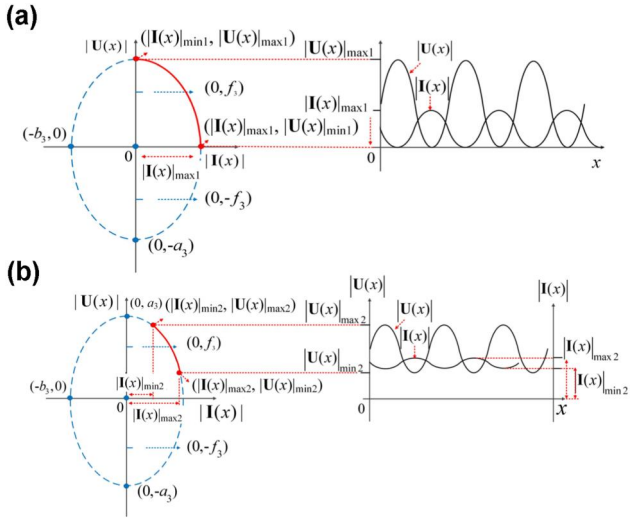

FIGURE 4 Ellipse diagram of Equation (19). (a) $\angle\mathbf{U}_2$-$\angle\mathbf{I}_2 = 90° \pm k \times 180°$, $k = 0, 1, 2, 3, \ldots$ (b) $\angle\mathbf{U}_2$-$\angle\mathbf{I}_2 \neq 90° \pm k \times 180°$, $k = 0, 1, 2, 3, \ldots$

Substitute Equation (24) into (21) to obtain maximum $|\mathbf{U}(x)|_{max1}$ as follows which is the peak value in Figure 4a at next page.

$$|\mathbf{U}(x)|^2_{max1} = a + \frac{1}{2}(b-a) + \sqrt{(0.5 \times c_{max})^2 + [0.5 \times (b-a)]^2} = a + b \quad (25)$$

In most cases, the maximum $|\mathbf{U}(x)|_{max2}$ can be derived by substituting Equation (23) into (21):

$$|\mathbf{U}(x)|^2_{max2} = \frac{1}{2}(b+a) + \frac{1}{2}\sqrt{4ab \times \sin(\theta_{\mathbf{U}_2} - \theta_{\mathbf{I}_2})^2 + (b-a)^2} \quad (26)$$

$|\mathbf{I}(x)|_{max2}$ can be derived in a similar process:

$$|\mathbf{I}(x)|^2_{max2} = \frac{1}{2}(e+d) + \frac{1}{2}\sqrt{4de \times \sin(\theta_{\mathbf{U}_2} - \theta_{\mathbf{I}_2})^2 + (e-d)^2} \quad (27)$$

As a result, once the $\angle\mathbf{U}_2$ and $\angle\mathbf{I}_2$ are known, the shape of $|\mathbf{U}(x)|-|\mathbf{I}(x)|$ ellipse is determined. It indicates that phase angle at busbar also affects in the weak positions in terms of maximum voltage or current harmonic levels in a system. Furthermore, the voltage and current maximum values are varying according to $\angle\mathbf{U}_2$-$\angle\mathbf{I}_2$ as Table 2 shown at next page. When the phase increases from 0° to 90°, maximum quantities of $|\mathbf{U}(x)|_{max}$ and $|\mathbf{I}(x)|_{max}$ vary from the lowest value to the highest one, which is monotonically increasing and when the phase decreases from 90° to 180°, $|\mathbf{U}(x)|_{max}$ and $|\mathbf{I}(x)|_{max}$ then decrease from the highest value to the lowest one, which is monotonically decreasing. The remaining two quadrants have the similar situation as Table 2 shown.

However, the maximum amplitudes of $|\mathbf{U}(x)|-|\mathbf{I}(x)|$ in power loss line are not fixed quantities, which is different from lossless line discussed in Section 2.1 when resistance and conductance of conductor cannot be ignored.

As a result, the $|\mathbf{U}(x)|-|\mathbf{I}(x)|$ plot does not strictly follow an elliptical formula since the maximum amplitudes are increasing when x increase gradually under the consumption that $\angle\mathbf{U}_2$-$\angle\mathbf{I}_2$ is known firstly. This situation is shown in Figure 5 in the next page.

TABLE 2 monotonic changing characteristic of maximum value of $|\mathbf{I}(x)|_{max}$ and $|\mathbf{U}(x)|_{max}$

$\angle\mathbf{U}_2$-$\angle\mathbf{I}_2$	[0°, 90°]	[90°, 180°]	[180°, 270°]	[270°, 360°]
$\|\mathbf{U}(x)\|_{max}$ and $\|\mathbf{I}(x)\|_{max}$	Monotonic increasing	Monotonic decreasing	Monotonic increasing	Monotonic decreasing

3 | ANALYSIS OF HARMONIC PROPAGATION USING U-I PLOT

As mentioned earlier, the analysis of harmonic propagation should not only focus on the harmonic levels at busbars, but also on the levels inside the power transmission lines, that is OHLs or UGCs. A **U-I** plot is proposed to analyse the harmonic propagation rule along the power lines.

3.1 | Discussion of harmonic orders

Assume harmonics at both terminals of power lines are measurable, then the situation that harmonics with specific orders have larger magnitudes within power lines than at the terminals is discussed below.

Harmonic voltage $\mathbf{U}(x)$ and current $\mathbf{I}(x)$ follow sinusoidal waveforms as Equation (7), and their wavelength can be calculated by (28):

$$\lambda_h = \frac{v_s}{f_h} \quad (28)$$

In the equation, λ_h is the wavelength for a specific harmonic, v_s is the velocity of the electric signal in the line and f_h is the frequency of the harmonic order. The velocity v_s can be calculated for a loss-less line as seen in (29) where C_0 is the speed of light, L_0 is the distributed inductance per unit length and C_0 is the distributed capacitance per unit length. According to (31), the harmonic angle at the busbar also influences the location of weak point alone the line. As a result, the wavelength, length of the line and the harmonic angle determine the existence of weak position between the two busses. Once the angle of the harmonic is known, the weak position along the line can be calculated by (31).

$$v_s = \frac{1}{c_0 \cdot \sqrt{L_0 \cdot C_0}} \quad (29)$$

3.2 | Weak positions in the power lines

The peak voltages or currents are more likely located at busbars for fundamental frequency or other low-order harmonic

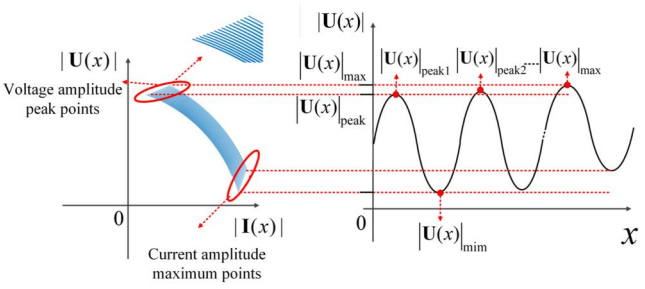

FIGURE 5 $|\mathbf{U}(x)|$-$|\mathbf{I}(x)|$ plot in power loss line

components due to its long wavelength, but less likely for high-frequency harmonic components. The weak position is referred to largest magnitudes of harmonic voltages and currents in all different harmonic orders along the power lines.

The weak positions along the power lines can be located based on the analysis below. As the frequency increases, the probability of occurrence of severe weak points in terms of high voltages or currents magnitudes increases because the wavelength decreases. After the first harmonic order with a peak value denoted as weak point is detected along the line, it is very likely that the next higher harmonic order components will also have the peak along the line, but with a different location.

Equation (31) can be calculated based on Equation (30) shown below, from which the distance from the busbar to weak point can be calculated, where x_I represents the distance from the ending bus when current magnitude $|\mathbf{I}(x)|$ reaches its maximum point and x_U represents the distance from the ending bus when voltage magnitude $|\mathbf{U}(x)|$ reaches its maximum point shown in Figure 4.

$$\begin{cases} |\mathbf{I}(x)|' = 0 \\ |\mathbf{U}(x)|' = 0 \end{cases} \tag{30}$$

$$\begin{aligned} x_I &= \frac{\arctan\left(\frac{-f}{e-d}\right)}{2\beta} \rightarrow I_{\max} \\ x_U &= \frac{\arctan\left(\frac{-c}{b-a}\right)}{2\beta} \rightarrow U_{\max} \end{aligned} \tag{31}$$

Different elliptic circles with various harmonic orders are shown in Figure 6, which illustrates the weak point of voltage and current along power line denoted by $|\mathbf{U}|_{\max}$ and $|\mathbf{I}|_{\max}$ represented by red dot in this figure in accordance with different harmonic orders. It can be readily seen that higher order harmonic components are more likely to have larger voltage and currents magnitudes along a transmission line or cable which is also illustrated in Figure 4b and the maximum voltage and current value can be easily found in this plot.

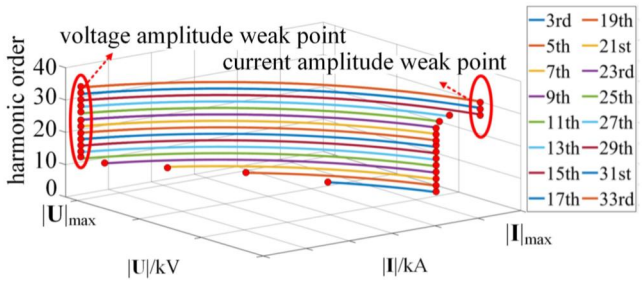

FIGURE 6 Three-dimensional |U|-|I| plot illustrating weak positions along power lines for different harmonic orders when L_0 and C_0 per km are frequency independent

This diagram also shows that when a peak value of a specific harmonic order component (e.g. 11th order) is detected beyond voltage limitation, the next higher orders components all have peak values beyond voltage standard. This is also suitable for harmonic current propagation situations as this figure shown.

4 | CASE STUDY

The proposed algorithm is then verified on a simple meshed benchmark system shown in Figure 7 and a bigger sized IEEE 39-bus test system shown in Figure 14 using MATLAB. The parameters of UGCs and OHLs included in the meshed system are shown in Tables 3 and 4 [21].

4.1 | 12-Bus test system

A harmonic emission source emits harmonic currents at a magnitude of 1 pu with angle 15° at Bus 1. Phase angle of voltage source G1 and G2 are 95° with voltage magnitude 1 pu. The base voltage is 138 kV and base current is 0.71 kA. The harmonic orders injected in the system are positive sequence harmonics of odd integers, up to the 41st harmonic order. Furthermore, only odd integers are included in order to give a resemblance to the harmonics present in a power system.

The resulting harmonic voltages at all 12 buses can be seen in Figure 8, when the harmonic emission source is implemented in Bus 1. As shown in Figure 8, harmonic voltage level in the 31st harmonic in Bus 5 is relatively higher than that of other buses in all harmonic orders. The reason is that when phase angle of various harmonic components at terminals are determined, bus five is the closest position to weak point as the trajectory shown in Figure 11. However, harmonic voltages in these buses are likely to be smaller than that along the power

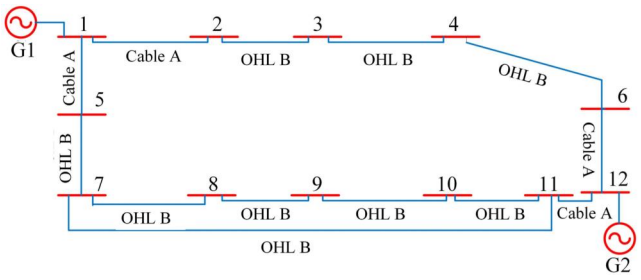

FIGURE 7 Single-line diagram of a meshed system

TABLE 3 Parameters of OHL A and B

	Resistance (Ω/km)	Inductance (mH/km)	Capacitance (μF/km)
Cable A	0.1262	0.3196	0.2109
OHL B	0.0186	0.9507	0.0123

lines shown in Figure 11. As a result, the weak point lies within power line other than buses.

The peak values of harmonic voltages at line from Bus 1-5-7 in the 31th order shown in Figure 9a is higher than voltages of Bus 1, Bus 5 marked with red arrow. This result can prove that harmonic voltage along the power line will be higher than that of buses when the weak point lies within the transmission line.

Figure 10 is the surface plot of the voltage propagation in the meshed system which could easily identify the area that includes weak point in the meshed system. According to Figure 10, the peak value of voltage occurs at line 1-five to seven at the 31th harmonic order, so the weak point can be identified to locate at power line within Bus 1 to Bus 7 through Bus 5. Finally, weak point can be accurately located using Equation (31).

TABLE 4 Power lines lengths

From bus	To bus	Length (km)
1	5	29
5	7	41.6
7	11	67.2
10	11	11
11	12	8.5
6	12	27.1
4	6	9.7
1	2	6.4
2	3	13.5
3	4	8.6
7	8	47.7
8	9	16.4
9	10	10

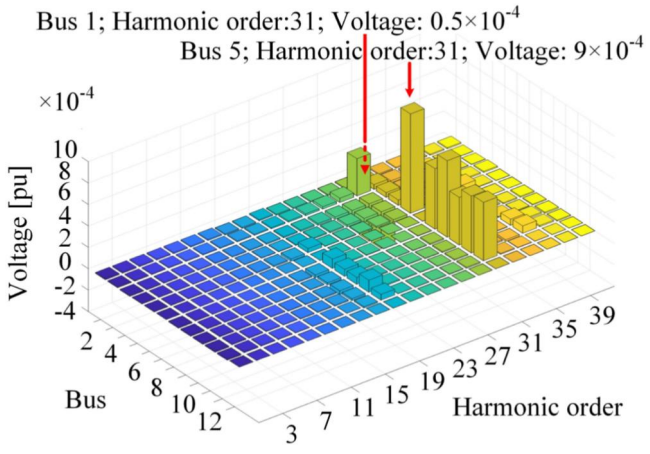

FIGURE 8 Harmonic voltage magnitudes in all the busses in the system, for all the harmonic order present, when a harmonic emission source is located at Bus 1

Clearer review of the harmonic voltage level of the 31th order throughout Bus 1 to Bus 7, can be seen in Figure 11, which is used as an example to explain how the harmonic voltage varies in more detail. The propagation follows the behaviour explained by the ellipse.

In Figure 11, the 31th harmonic voltage moves from starting point Bus 1 to Bus 7 and reaches its maximum point denoted by the weak position along the power line. This sinusoidal amplification in magnitude demonstrates the

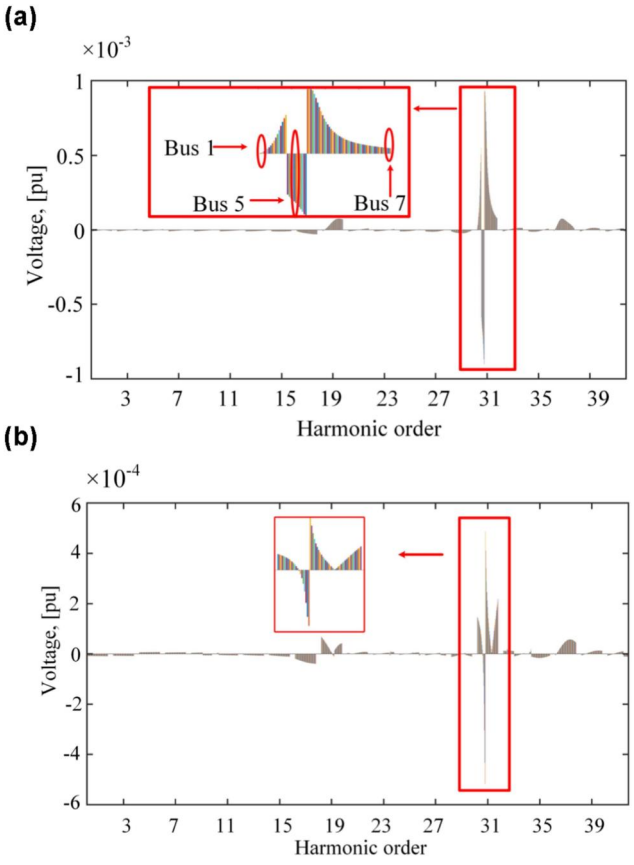

FIGURE 9 Voltages along the power lines in the meshed system. Negative voltage indicates a voltage phase-shift. (a) Voltage along the line from Bus 1 to Bus 7 through Bus 5 (b) Voltage along the line from Bus 7 to Bus 9 through Bus 8

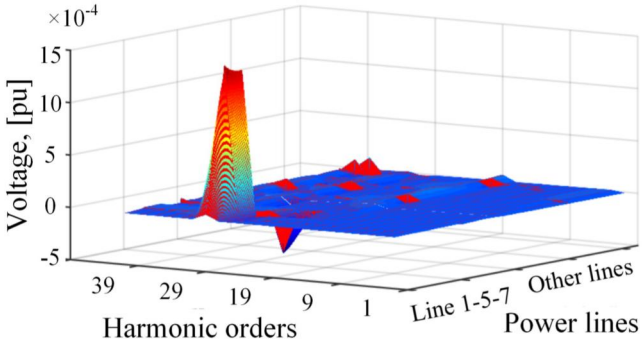

FIGURE 10 Three-dimensional plot of the voltage propagation in the meshed system

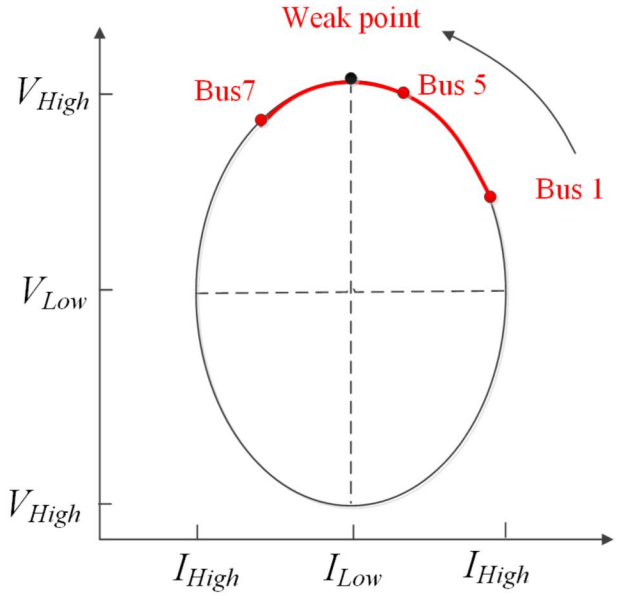

FIGURE 11 Illustration of the 31th harmonic voltage along a long line

importance of the measuring point at which the harmonic level is measured, as the RMS value of the harmonics are different at different locations throughout a line. As a result, whether the weak point exists in a certain harmonic order can be found according to U–I plot as shown in Figure 11 and a 3-dimensional $|\mathbf{U}|$-$|\mathbf{I}|$ plot illustrating weak positions from Bus 1 to Bus seven in different harmonic orders is shown as follows.

As shown in Figure 12, lower harmonic orders like 3rd–29th do not likely contain maximum voltage value while the weak point lies within 31st–33rd harmonic orders. The reason is that when phase angle of voltage and current are known to be specific values, 95° of voltage angle and 15° of current angle in this case introduced above, the only impact factors are harmonic order and power line length, and the length of the cable connected between Bus 1 and Bus 5 is closer to quarter of the wavelength of the 31st and 33rd harmonic order while lower harmonic orders are in accordance with longer wavelength λ_b calculated in (28). As a result, the voltage weak point can be derived in 31th harmonic order as shown in Figure 12 and the location of it can be calculated using (31). Moreover, if the line is long enough to be a quarter length, there is always a maximum voltage or current along the line, for example for the 31th and 33rd-harmonic as discussed above. However, there can also be one the maximums even if the line is smaller than a quarter of wavelength, depending on the starting point which is based on the angle and magnitude of harmonic injection according to (18).

The weak point identification method is tested in PSCAD based on Figure 7. A 31th-0.72 kA harmonic source with phase angle 15° locates at Bus 1. The voltage sources G1, G2 are 138kV and the phase angle of them is set to be 95°. According to (31), the voltage weak point lies within the cable line Bus 1–Bus 5 which is 29 km from harmonic source (G1 connected

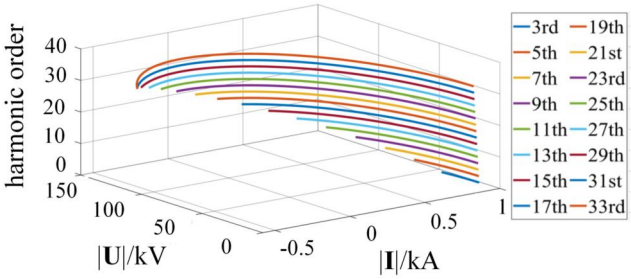

FIGURE 12 Three-dimensional $|\boldsymbol{U}|$-$|\boldsymbol{I}|$ plot illustrating weak positions along power line in different harmonic orders: first- 33rd

Bus), and Figure 13c verifies it as the voltage at 29 km from Bus 1 is 290 kV larger than any other voltages at buses or transmission line.

4.2 | IEEE 39-bus test system

To further prove the effectiveness of the proposed weak positions identification in terms of maximum harmonic levels in a larger power system with multiple harmonic orders being injected simultaneously, an IEEE 39-bus system shown in Figure 14 is simulated in MATLAB to study the ellipse relationship between spatial harmonic voltages and currents and identify the weak position, finally, the weak position calculated from Equation (31) is proved in PSCAD.

Two harmonic current sources located at Bus 23 and Bus 21 contain the third, ninth, 13th and 19th orders' components with amplitudes of 0.01 kA and phase angle 0°. Phase angle of Generator 7 is set to be 90° and other generators are set according to benchmark parameters, which are the known values. The harmonic power flow that may result in the existence of weak positions along AC power lines are marked with yellow arrows in Figure 14. The length of Lines 31 and 32 are modified to be 60 km to show the harmonic voltage propagation along the power lines. All other parameters are set according to benchmark model in Ref. [22] in which the lengths of Lines 33, 32, 31 and 30 are 37, 60, 60 and 30 km. Lines 30–33 that connect to harmonic sources are chosen as an example. Once the harmonic angles and amplitudes at terminals are known, four different three-dimensional plots of voltage propagation of four power lines are shown in Figure 15 below in which line 32 and 33 depicted in (a) and (b) will have weak positions that maximum voltages along lines reach 1.5 pu in accordance with specific harmonic order and power line length. The base values of voltages and currents are terminal harmonic voltages and harmonic current injection amplitude (0.01 kA). Finally, weak point can be accurately located using Equation (31).

Clearer review of the harmonic voltage and current level of different orders of lines 30-33 can be seen in Figure 16, which is used as an example to explain how the harmonic voltage and current varies in more detail.

Note that the voltage weak points locate at Lines 32 and 33, shown in Figure 15a,b, when the angle difference of voltage

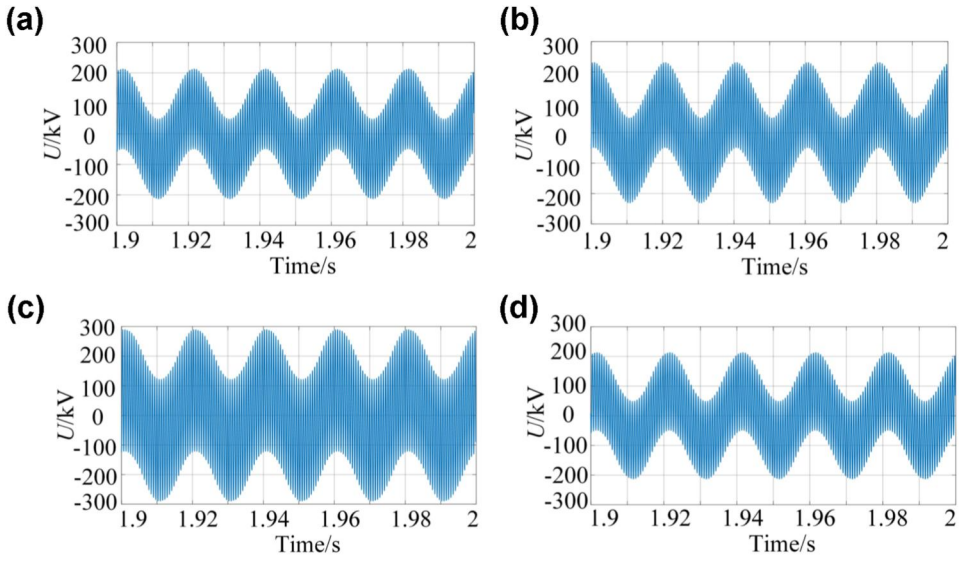

FIGURE 13 Phase a to ground voltage measured at different location from the harmonic source at bus 1 within the power line from bus 1 to bus 7. (a) 5 km from Bus 1, (b) 15 km from Bus 1, (c) 29 km from Bus 1, (d) 50 km from bus 1

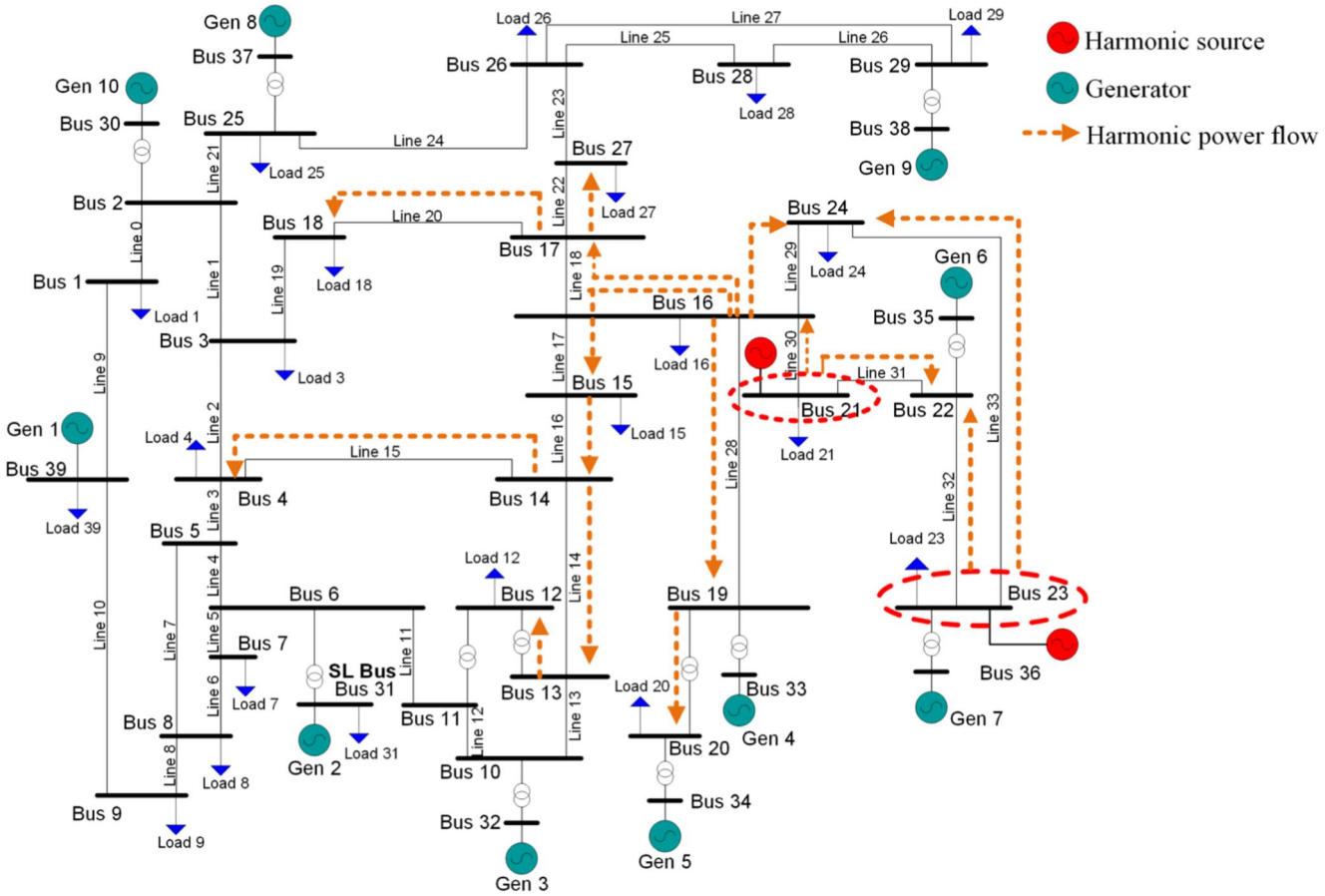

FIGURE 14 IEEE 39-bus system

and current at terminal: Bus 22 and Bus 24 reaches 90°. The same situations can be proved in Figure 16a,b that maximum voltages reach 1.2 or 1.5 pu in the 15th and above harmonics or the ninth and above harmonics, respectively, which referred to voltage weak points. Meanwhile, the maximum currents of line 33 and 32 also reach their maximum point of 1.2 or 1.5 pu,

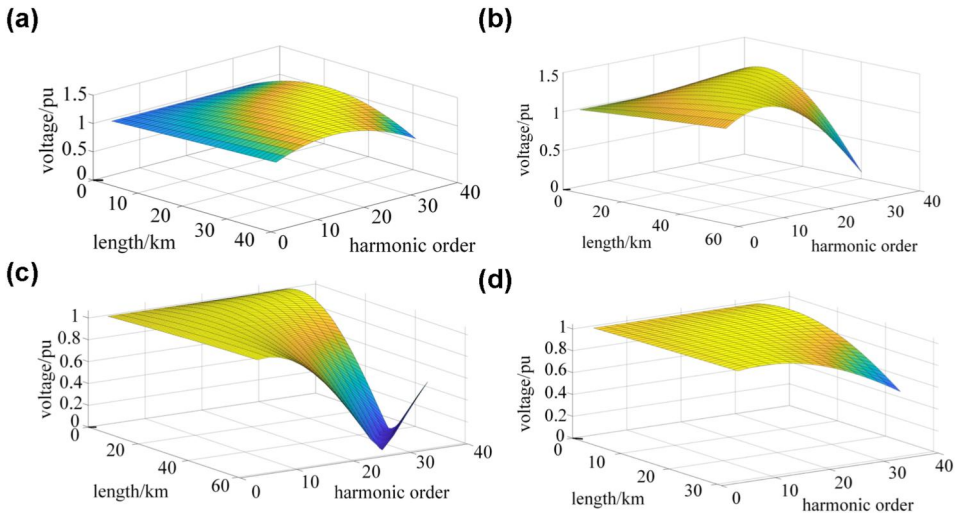

FIGURE 15 Three-dimensional plot of the voltage propagation in IEEE 39-bus system (a) Line 33, (b) Line 32, (c) Line 31, (d) Line 30

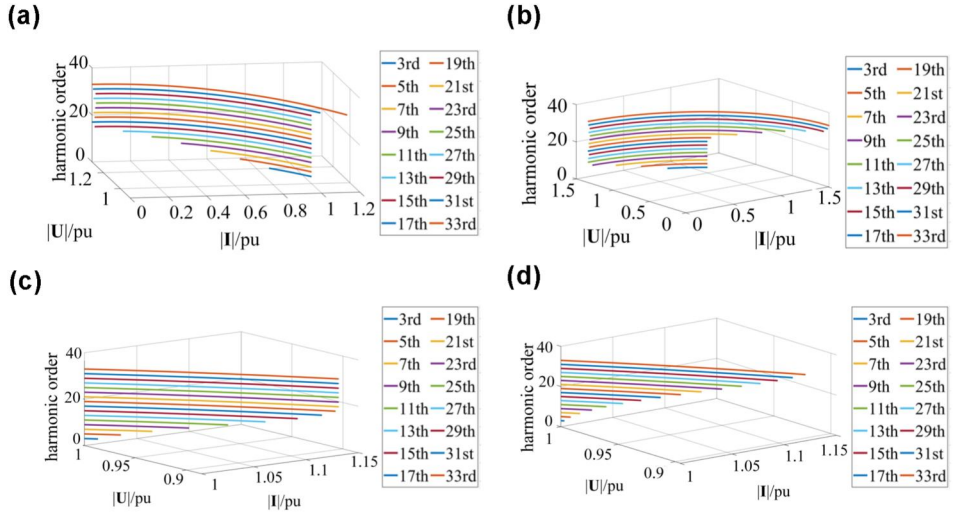

FIGURE 16 Three-dimensional $|\mathbf{U}|$-$|\mathbf{I}|$ plot illustrating weak positions along power lines in different harmonic orders: first–33rd. (a) Line 33, (b) Line 32, (c) Line 31, (d) Line 30

respectively, in the 33rd and above harmonics or the 27th and above harmonics that are referred to as current weak points. In contrast, as shown in Figures 15c,d and 16c,d that the angle difference of terminal harmonic voltage and current are set to be zero, the maximum voltage along power lines 31 and 30 will be the smallest one according to Equation (26). As a result, the voltage weak point does not locate at line 31 and 30. Similarly, according to Equation (27) and Figure 16c,d, the maximum currents in different harmonic orders are also the smallest ones that current weak point does not likely to locate at line 31 and 30.

The weak point identification method is tested in PSCAD. According to the analysis before, the voltage weak points lie within the power line 32 and 33. Taking line 33 for an example that the voltage weak point for the 19th harmonic component is calculated to be 10 km from harmonic source at Bus 23 based on Equation (31), and Figure 17c verifies it as the harmonic voltage with the 19th order at 10 km from Bus 23 is 27.5 kV larger than any other voltages at buses or transmission line.

4.3 | Discussion of obtained results and main achievements

The correctness of the proposed elliptical model-based three impact factors, which influence the weak points existence and weak positions along power lines, is verified in the MATLAB and PSCAD using 12-bus meshed system and IEEE 39-bus test system.

The impact factors (i) and (ii), that is harmonic orders and power line lengths, which determine the weak positions in terms of harmonic voltages and currents, are simulated and verified on 12-bus meshed system. In this simulation, the

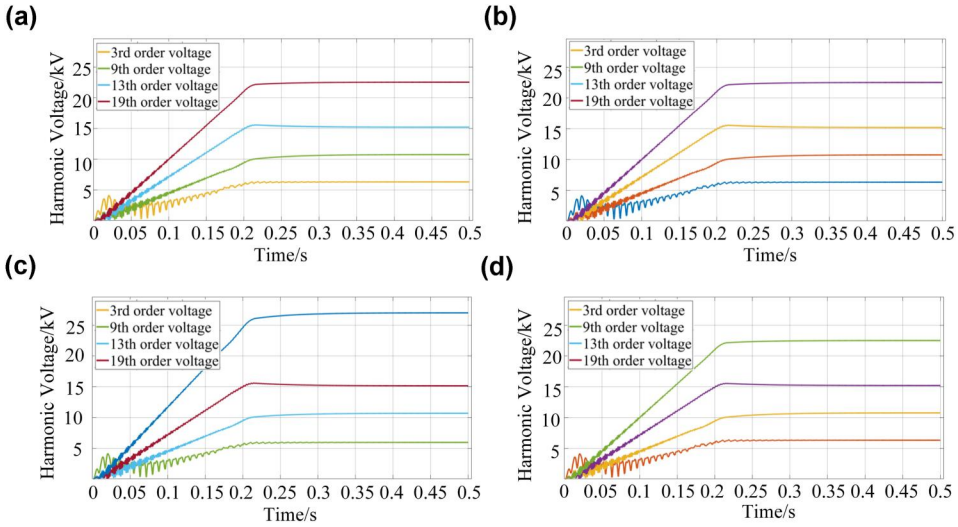

FIGURE 17 Phase a to ground voltage measured at different location from the harmonic source at Bus 23 within the power line 33. (a) 37 km from Bus 23, (b) 20 km from Bus 23, (c) 10 km from Bus 23, (d) 0 km from Bus 23

harmonics with higher orders and the line lengths in accordance with quarter of the wavelength of harmonics are proved to be two impact factors that determine the weak positions along the power lines.

The impact factors (iii), that is phase angle differences of harmonic voltages and currents at terminals of power lines, are proved to be a significant aspect that determines the existence of the weak points along power lines. Its correctness is verified on the IEEE 39-bus system by setting different phase angle differences of harmonics. In general, the weak points are more likely to exist when the phase angle differences approach to 90° or 270°.

5 | CONCLUSION

This paper proposes a novel elliptic model to evaluate the harmonic propagation along the power line between busbars. From the model, an elliptic formula of harmonic **U-I** plot is proved using analytical geometry and the harmonic waveforms including voltage and current along the line are proved to match with sinusoidal waveform and simulated based on MATLAB. It is observed that the maximum amplitude of voltage and current along AC power lines depends on (i) voltage and current harmonic orders at terminals of line; (ii) power line length; (iii) the steady-state harmonic angle difference of voltage and current. Factor (iii) influences the maximum values of harmonic voltage and current, and Factors (i) and (ii) determine weak position in terms of harmonic voltage and current. Furthermore, for a lossy power line, the maximum value of voltage and current along the transmission lines are decided by the angle difference between voltage and current at terminals as well as the real part of propagation coefficient. All in all, the feature scope of this paper aims at solving two problems for system operator: (1) The existence of voltage and current weak points along specific power lines; (2) Weak position along power lines.

Future works include studying the influences from nonlinear transformer of weak point identification and studying the filter optimal allocation considering harmonic amplification along power lines.

ACKNOWLEDGEMENT

National Natural Science Foundation of China: 52007133.

CONFLICT OF INTEREST

No conflict of interest exits in the submission of this manuscript.

DATA AVAILABILITY STATEMENT

Data sharing is not applicable to this article as no new data were created or analysed in this study.

ORCID

Chengxi Liu https://orcid.org/0000-0003-0262-5314
Zhen Gong https://orcid.org/0000-0002-6037-2995
Filipe Faria da Silva https://orcid.org/0000-0002-2640-0964
Qiupin Lai https://orcid.org/0000-0002-1500-8684
Pan Hu https://orcid.org/0000-0003-1952-0666

REFERENCES

1. Energinet: Energinet analysis assumption, p. 60. Erritsø (DK): Energinet.dk (2017)
2. IEEE: IEEE recommended practice and requirements for harmonic control in electric power systems, p. 29. IEEE Power and Energy Society, New York (2014). https://ieeexplore.ieee.org/servlet/opac?punumber=6826457
3. Da Silva, F.F.: Analysis and simulation of electromagnetic transients in HVAC cable transmission grids, PhD thesis, Aalborg University (2011)
4. Jensen, C.F.: Harmonic background amplification in long asymmetrical high voltage cable systems. Electr. Power Syst. Res. 160, 292–299 (2018)
5. Energinet, dk: Technical issues related to new transmission lines in Denmark - west coast line from German border to Edrup and Endrup-Idomlund, p. 132. Energinet.dk (2018)

6. Escudero, M.V., et al.: Network Modelling for Harmonic Studies, Technical Brochures. CIGRE (2019) [Cited 2021 Feb 19]. https://e-cigre.org/publication/766-network-modelling-for-harmonic-studies
7. Fillion, Y., Deschanvres, S.: Background harmonic amplifications within offshore wind farm connection projects. In: Proceedings of the International Conference on Power System Transients, pp. 1–8. Cavtat, Croatia (2015)
8. Velitsikakis, K., et al.: Challenges and mitigations for the energization of large offshore grids in the Netherlands. In: Proceedings of International Conference on Power System Transients, pp. 1–6. Perpignan, France (2019)
9. Kwon, J.B., Hansen, C.S., Flytkjær, C.F.: System-wide amplification of background harmonics due to the integration of high voltage power cables. In: Proceedings of CIGRE Paris Session, Paper c4-305. (2020)
10. Cunniffe, N., et al.: Investigating the methodology and implications of implementing long HVAC cables in the Ireland and northern Ireland power system. In: Proceedings of CIGRE Paris Session, paper C4-208. (2016)
11. Li, Z., et al.: Quantitative severity assessment and sensitivity analysis under uncertainty for harmonic resonance amplification in power systems. IEEE Trans. Power Deliv. 35(2), 809–818 (2020)
12. He, J., et al.: Analysis and mitigation of resonance propagation in grid-connected and islanding microgrids. IEEE Trans. Energy Convers. 30(1), 70–81 (2015)
13. Li, Z., et al.: A rapid modal analysis method for harmonic resonance using modified power iteration. IEEE Trans. Power Deliv. 33(3), 1495–1497 (2018)
14. Wright, P.S., et al.: Multiple-site amplitude and phase measurements of harmonics for analysis of harmonic propagation on Bornholm Island. IEEE Trans. Instrum. Meas. 66(6), 1176–1183 (2017)
15. Bompard, E., Carpaneto, E., Napoh, R.: Survey of harmonic distortion in LV and MV networks: results and corrective strategies. In: Proceedings of the 16th International Conference and Exhibition on Electricity Distribution, pp. 18–21. (2001)
16. Wikipedia [Internet]. Telegrapher's Equation. [Updated 2021 January 14, Cited 2021 April 10]; [About 4 screens]. (2001). https://en.wikipedia.org/wiki/Telegrapher's_equations
17. Wikipedia [internet].McCammon, R.: SPICE Simulation of Transmission Lines by the Tele-grapher's Equations into a Circuit (2001). [Updated 2010 June, Cited 2021 April 10]. http://i.cmpnet.com/rfdesignline/2010/06/C0580Pt1edited.pdf
18. Cvetićanin, S.M., Rapaić, M.R., Zorica, D.: Frequency analysis of generalized time-fractional telegrapher's equation. In: Proceedings of 2017 European Conference on Circuit Theory and Design (ECCTD), Catania, pp. 1–4. (2017)
19. Singh, B., Singh, S.: GA-based optimization for integration of DGs, STATCOM and PHEVs in distribution systems. Energy Rep. 5, 84–103 (2019)
20. Ali, E.S., Abd Elazim, S.M., Abdelaziz, A.Y.: Ant lion optimization algorithm for renewable distributed generations. Energy. 116, 445–458 (2016)
21. Lennerhag, O.: Power System Model for Resonance Studies [internet]. Luleå University of Technology, Luleå (2018). Cited 2021 April 10. http://www.diva-portal.org/smash/get/diva2:1249815/FULLTEXT02.pdf
22. PSCAD. IEEE 39 Bus System [Internet]. Manitoba Hydro International Ltd. (MHI), Manitoba, CA (2018). Cited 2021 April 10. https://www.pscad.com/knowledge-base/download/ieee_39_bus_technical_note.pdf

How to cite this article: Liu, C., et al.: A study of harmonic spatial propagation along AC power lines of meshed power systems. IET Circuits Devices Syst. 1–13 (2021). https://doi.org/10.1049/cds2.12107